Available online at www.sciencedirect.com

SCIENCE @ DIRECT®

International Journal of Heat and Fluid Flow 26 (2005) 780–791

International Journal of
HEAT AND FLUID FLOW

www.elsevier.com/locate/ijhff

Variable property, steady, axi-symmetric, laminar, continuum plasma flow over spheroidal particles

Yuemin Wen, Milind A. Jog *

Department of Mechanical, Industrial, and Nuclear Engineering, P.O. Box 210072, 687 Rhodes Hall, University of Cincinnati, Cincinnati, OH 45221-0072, United States

Received 30 August 2004; accepted 29 January 2005
Available online 23 March 2005

Abstract

Steady, continuum, laminar plasma flow over spheroidal particles has been numerically investigated in this paper using a finite volume method. To body-fit the non-spherical particle surface, an adaptive orthogonal grid is generated. The flow field and the temperature distribution are calculated for oblate and prolate particle shapes. A number of particle surface temperatures and far field temperatures are considered and thermo-physical property variation is fully accounted for in our model. The particle shapes are represented in terms of axis ratio which is defined as the ratio of axis perpendicular to the flow direction to the axis along the flow direction. For oblate shape, axis ratios from 1.6 (disk-like) to 1 (sphere) are used whereas for prolate shape, axis ratios of 1(sphere) to 0.4 (cylinder-like) are used. Effects of flow Reynolds number, particle shape, surface and far field temperatures, and variable properties, on the flow field, temperature variations, drag coefficient, and Nusselt number are outlined. Results show that particle shape has significant effect on flow and heat transfer to particle surface. Compared to a constant property flow, accounting for thermo-physical property variation leads to prediction of higher temperature and velocity gradients in the vicinity of the particle surface. Based on the numerical results, a correlation for the Nusslet number is proposed that accounts for the effect of particle shape in continuum flow with large thermo-physical property variation.

Keywords: Heat transfer; Non-spherical particles; Variable properties; Numerical analysis

1. Introduction

Plasma flow over small powder particles is encountered in many thermal plasma aided manufacturing processes (Smith et al., 1989). Due to the small size of the particles, the Reynolds number based on particle diameter may be in the intermediate regime (*Re* = 10–100). The particle surface temperature is close to its melting temperature (~1000–3000 K), and away from the particle surface, within a relatively short distance, temperature reaches the free stream temperature (>10,000 K). Consequently the thermo-physical properties may change by an order of magnitude in the flow field around a particle. As a result the flow and temperature variation around a particle injected in thermal plasma flow can be quite different from that of a particle injected in a gas flow where thermo-physical property variation is relatively small. Furthermore, powder particles typically injected in plasma spray system may not be spherical. Hence the effect on heat transfer due to non-spherical particle shape with large thermo-physical property variation in the flow field needs to be investigated.

Due to their importance in spray systems, flow over solid and liquid particles has received extensive attention in published literature. Monographs by Clift et al.

---

* Corresponding author. Tel.: +1 513 556 1675; fax: +1 513 556 3390.
E-mail address: milind.jog@uc.edu (M.A. Jog).

0142-727X/$ - see front matter © 2005 Elsevier Inc. All rights reserved.
doi:10.1016/j.ijheatfluidflow.2005.01.002

Nomenclature

a	particle diameter perpendicular to the flow
b	particle diameter in the direction of the flow
c_p	specific heat at constant pressure, J/kg k
d	sphere diameter
f	grid cell aspect ratio
h	heat transfer coefficient, W/m^2 K
H_ξ, H_η, H_ϕ	metric coefficients for ξ, η, ϕ directions
I	the unit tensor $\begin{bmatrix}1 & 0 & 0\\ 0 & 1 & 0\\ 0 & 0 & 1\end{bmatrix}$
k	fluid thermal conductivity, W/m k
P	pressure, N/m^2
T	temperature, K
u	flow velocity, m/s
Dimensionless numbers	
C_d	drag coefficient drag force/($0.5\rho_\infty U_\infty^2 \times$ projected area)
Nu	Nusselt number ha/k_∞
Pr	Prandtl number $\mu_\infty c_{p\infty}/k_\infty$
Re	Reynolds number $U_\infty a/\nu_\infty$
Sh	Sherwood number
Greeks	
ρ	density, Kg/m^3
μ	dynamic viscosity, N s/m^2
ν	kinematic viscosity, m^2/s
π	stress
ξ, η, ϕ	coordinates for the orthogonal body-fitted grid
Subscripts	
wall	particle surface
∞	far field conditions
Superscript	
t	transpose

(1978) and Sadhal et al. (1997) provide extensive reviews of experimental, numerical, and analytical work on fluid flow over spherical and non-spherical drops as well as particles and the concomitant heat and mass transfer. In majority of the spray applications, the particles are small and the flow over the particles is laminar. The laminar flow over solid spherical particles can be divided into three regimes (Sadhal et al., 1997). First is low Re regime ($0 < Re < \sim 20$) where the flow tends to conform to the particle surface. There is no flow separation at the rear of the particle. The local heat or mass transfer coefficient (or local Nusselt or Sherwood number) decreases monotonically from the front stagnation point to the rear. In the intermediate Re regime ($20 < Re < \sim 140$) a recirculatory toroidal vortex is formed near the rear stagnation point. Due to flow recirculation, fluid with temperature (or concentration) close to free stream temperature (or concentration) is brought closer to the rear surface of the droplet and the local Nusselt number or Sherwood number increases near the rear stagnation point. At $Re > \sim 140$ the flow becomes unsteady and Re of about 400 vortex shedding with regular frequency takes place. Correlations for drag coefficient and Nusselt or Sherwood number for spherical particles exposed to a constant property flow for Re up to 400 are provided in Clift et al. (1978) and for liquid drops in Ayyaswamy (1995).

Numerical solutions for flow field and heat/mass transfer from spheroids exposed to steady, constant property flow have been reported by Masliyah and Epstein (1970); Comer and Kleinstreuer (1995a and 1995b), and Chuchottaworn and Asano (1986), among others. Their results show that the surface pressure variation and local Nusselt number and consequently the drag coefficient and overall Nusselt number are a strong function of the aspect ratio for oblate and prolate spheroids. At low Reynolds number, the total drag on an oblate spheroid is higher for oblate spheroid with lower aspect ratio (closer to 1). However, at higher Reynolds number, ($Re >$ about 50), oblate spheroids with higher aspect ratio have higher total drag coefficient. Though the local mass (heat) transfer shows a fairly complicated variation with aspect ratio at a given Reynolds number, the average Nusslet number increases with increasing aspect ratio. Chuchottaworn and Asano (1986) proposed a correlation to predict the average Nusselt number for constant property flow over non-spherical particles that matched their results within ±5%.

Boulos et al. (1994) provide a review of processes that take place in plasma flow. Considerable studies of heat transfer to particles in plasma flow are available. Reviews by Chyou and Pfender (1989) delineate the different heat transfer processes and provide correlations for mass and momentum transfer to spherical particles in plasma flow. Plasma systems typically involve temperatures that are as high at 15,000 K. With particle surface temperature being close to its melting temperature, very high temperature gradients and corresponding property variations of over an order of magnitude may be present in a short distance around the particle. Furthermore, for very small particles, non-continuum effect can become important. Free-molecular flow and non-continuum flow over particles has been extensively investigated by

Chen and co-workers (Chen, 1997; Chen et al., 1994) and Gnedovets and Uglov (1992). The effect of thermo-physical property variation on heat conduction to a stationary spherical particle has been investigated using an integral heat conductivity approach by Bourdin et al. (1983). This approach was later extended by Joshi et al. (1986) to account for property variations and non-continuum effects on mass transfer from a stationary particle in plasma. Additionally, due to gas ionization at high temperatures, the particle is negatively charged and the flow of ions and electrons to the particle surface contributes to the heat transfer (Ayyaswamy and Cohen, 2002; Jog and Huang, 1996; Hader and Jog, 1998). Also, there may be some degree of evaporation from particle surface. Non-continuum effects, ionization, and evaporation effects have not been considered in the present paper. Based on limited experimental data, several correlations have been proposed for Nusselt number for a spherical particle. As shown by Young and Pfender (1987), the predictions by different correlations agree well at lower temperatures. However, at high temperatures, there is no unanimity in the predicted values by the correlations. A numerical study of variable property plasma flow over a spherical particle was carried out by Sayegh and Gauvin (1979). However, they report negative drag coefficients at $Re = 50$ and it is unclear whether the results are reliable at higher Reynolds number.

In this paper we have considered continuum plasma flow over non-spherical particles. Effects of particle shape and thermo-physical property variation on the convective heat transfer have been investigated. Non-continuum effects, ionization, and evaporation effects are not considered in the numerical analysis.

2. Solution methodology

The governing equations are the mass conservation, momentum conservation, and energy conservation equations. The heating of a particle in plasma flow is a transient process with possible phase change at the interface. Following assumptions are made to simplify the analysis. Steady state heat transport is considered in the gas phase. As the ratio of heat capacities of the gas to the particle is very small $\sim 0\ (10^{-3})$, the time scale for particle heating is much larger than the time scale for transport in the gaseous phase. Therefore a quasi-steady approach can provide accurate results (Chyou and Pfender, 1989; Jog and Huang, 1996). In this approach, the transport in the gas phase is determined by time independent equations. If required, the transient variation of the particle temperature can be obtained, using the steady-state gas phase heat transfer results at each time step. As the focus of this study is to understand the effect of particle shape on the transport, the transient particle temperature variations are not obtained. Also, phase change at the particle surface has not been considered in this analysis. Only the gas phase analysis has been carried out. In a plasma spray, particle–particle interactions may influence the rate of momentum and heat transport. Correlations are available that incorporate particle–particle interaction effects on the heat transfer as a correction to Nusselt number for a single particle (Verma and Jog, 2000). Therefore, it is important to accurately determine the heat transfer to a single particle before corrections for particle–particle interactions can be used. As such, particle–particle interactions are not considered in the present analysis. Governing continuum conservation equations for steady, variable property flow over a particle with no body forces and negligible viscous dissipation can be written as:

Mass conservation:

$$\nabla \cdot (\rho \vec{u}) = 0 \tag{1}$$

Momentum conservation equation:

$$\rho (u \cdot \vec{\nabla}) \vec{u} = \nabla \cdot \vec{\pi} \tag{2}$$

where the stress $\vec{\pi} = -p\vec{I} + \mu[\nabla \vec{u} + (\nabla \vec{u})^{\mathrm{t}} - \frac{2}{3}\vec{I}(\nabla \cdot \vec{u})]$

Energy conservation equation:

$$\rho c_p \vec{u} \cdot \nabla T = \nabla \cdot (k \nabla T) - \frac{T}{\rho}\left(\frac{\partial \rho}{\partial T}\right)_{\mathrm{p}} \vec{u} \cdot \nabla p \tag{3}$$

These equations are solved using a finite volume method. The boundary conditions include specified uniform far field temperature and velocity, no-slip condition and specified temperature at the particle surface, axi-symmetry condition along the centerline. The thermo-physical property variations for the gas are taken from Boulos et al. (1994).

Since we consider non-spherical particle shapes, it is desirable to solve the governing equations using a body fitted grid. Furthermore, orthogonal grids have lower truncation errors and produce more stable solutions than those obtained with non-orthogonal grids. Also, the governing equations obtained by using an orthogonal co-ordinate system are much simpler than those obtained with a non-orthogonal system. For these reasons, we have used an orthogonal body-fitted grid that is generated using method outlined by Eca (1996). Note that only a two-dimensional grid needs to be obtained as the flow is assumed to be axi-symmetric. Here (ξ, η) coordinates in the computational domain map the (x, y) coordinates in the physical domain.

2.1. Orthogonal mapping

A two-dimensional (2D) orthogonal grid satisfies the condition:

$$g_{\xi\eta} = x_\xi x_\eta + y_\xi y_\eta = 0 \tag{4}$$

where the quantity $g_{\xi\eta}$ is proportional to the cosine of the angle between a coordinate line along the ξ direction and a coordinate line along the η direction. The grid cell aspect ratio (or distortion function), f is defined as $f = \frac{H_\eta}{H_\xi}$ where H_η and H_ξ are the scale factors defined as

$$\begin{aligned} H_\eta &= \sqrt{g_{\eta\eta}} = \sqrt{x_\eta^2 + y_\eta^2} \\ H_\xi &= \sqrt{g_{\xi\xi}} = \sqrt{x_\xi^2 + y_\xi^2} \end{aligned} \tag{5}$$

Note that the quantities, $\sqrt{g_{\xi\xi}}$ and $\sqrt{g_{\eta\eta}}$ are proportional to the arc lengths along ξ and η directions, respectively. The governing equations for mesh generation can now be derived by considering the Beltrami equations (Thompson and Warsi, 1982),

$$\begin{aligned} \frac{\partial x}{\partial \eta} &= -f\frac{\partial y}{\partial \xi} \\ \frac{\partial y}{\partial \eta} &= f\frac{\partial x}{\partial \xi} \end{aligned} \tag{6}$$

where f, the distortion function, is a positive quantity.

It can be seen that if x and y satisfy the Beltrami equations (Eq. (6)) then they also satisfy the orthogonality criterion (Eq. (4)). Therefore, using Beltrami equations and the equalities,

$$\begin{aligned} \frac{\partial}{\partial \eta}\left(\frac{\partial x}{\partial \xi}\right) &= \frac{\partial}{\partial \xi}\left(\frac{\partial x}{\partial \eta}\right) \\ \frac{\partial}{\partial \eta}\left(\frac{\partial y}{\partial \xi}\right) &= \frac{\partial}{\partial \xi}\left(\frac{\partial y}{\partial \eta}\right) \end{aligned} \tag{7}$$

a set of coupled, non-linear partial differential equations for generating the mesh can be obtained as

$$\left.\begin{aligned} \frac{\partial}{\partial \xi}\left(f\frac{\partial x}{\partial \xi}\right) + \frac{\partial}{\partial \eta}\left(\frac{1}{f}\frac{\partial x}{\partial \eta}\right) &= 0 \\ \frac{\partial}{\partial \xi}\left(f\frac{\partial y}{\partial \xi}\right) + \frac{\partial}{\partial \eta}\left(\frac{1}{f}\frac{\partial y}{\partial \eta}\right) &= 0 \end{aligned}\right\} \tag{8}$$

The solution of Eq. (8) provides the orthogonal grid. These equations can be discretized by applying the 'control volume' approach and using second order accurate central differencing. The resulting algebraic equations are solved using a point iterative under relaxation method. The solution is considered convergent when the maximum relative difference in f at any grid point between successive iterations is below 1×10^{-4} and the maximum deviation from orthogonality from two grid lines is below 0.1 (Wen, 2004).

The governing equations are written in the orthogonal curvilinear coordinates (ξ, η, ϕ). Note that due to the axi-symmetric nature of the problem, $\partial/\partial\phi = 0$ and $u_\phi = 0$.

Continuity equation

$$\frac{\partial(\rho H_\eta H_\phi u_\xi)}{\partial \xi} + \frac{\partial(\rho H_\xi H_\phi u_\eta)}{\partial \eta} = 0 \tag{9}$$

Momentum equation

$$\begin{aligned} &\frac{u_\xi}{H_\xi}\frac{\partial u_\xi}{\partial \xi} + \frac{u_\eta}{H_\eta}\frac{\partial u_\xi}{\partial \eta} + \frac{u_\xi u_\eta}{H_\xi H_\eta}\frac{\partial H_\xi}{\partial \eta} - \frac{u_\eta^2}{H_\xi H_\eta}\frac{\partial H_\eta}{\partial \xi} \\ &\quad = \frac{1}{\rho}\left\{\frac{1}{H_\xi H_\eta H_\phi}\left(\frac{\partial}{\partial \xi}(H_\eta H_\phi \pi_{\xi\xi}) + \frac{\partial}{\partial \eta}(H_\phi H_\xi \pi_{\xi\eta})\right)\right. \\ &\qquad \left. + \frac{\pi_{\xi\eta}}{H_\eta H_\xi}\frac{\partial H_\xi}{\partial \eta} + \frac{\pi_{\xi\phi}}{H_\phi H_\xi}\frac{\partial H_\xi}{\partial \xi} - \frac{\pi_{\eta\eta}}{H_\eta H_\xi}\frac{\partial H_\eta}{\partial \xi} - \frac{\pi_{\phi\phi}}{H_\phi H_\xi}\frac{\partial H_\phi}{\partial \xi}\right\} \\[2ex] &\frac{u_\xi}{H_\xi}\frac{\partial u_\eta}{\partial \xi} + \frac{u_\eta}{H_\eta}\frac{\partial u_\eta}{\partial \eta} + \frac{u_\xi u_\eta}{H_\xi H_\eta}\frac{\partial H_\eta}{\partial \xi} - \frac{u_\xi^2}{H_\xi H_\eta}\frac{\partial H_\xi}{\partial \eta} \\ &\quad = \frac{1}{\rho}\left\{\frac{1}{H_\xi H_\eta H_\phi}\left(\frac{\partial}{\partial \xi}(H_\eta H_\phi \pi_{\xi\eta}) + \frac{\partial}{\partial \eta}(H_\phi H_\xi \pi_{\eta\eta})\right)\right. \\ &\qquad \left. + \frac{\pi_{\xi\eta}}{H_\eta H_\xi}\frac{\partial H_\eta}{\partial \xi} - \frac{\pi_{\xi\xi}}{H_\eta H_\xi}\frac{\partial H_\xi}{\partial \eta} - \frac{\pi_{\phi\phi}}{H_\phi H_\eta}\frac{\partial H_\phi}{\partial \eta}\right\} \end{aligned} \tag{10}$$

where

$$\pi_{\xi\xi} = -p - \frac{2}{3}\mu\nabla\cdot\vec{u} + 2\mu\left(\frac{1}{H_\xi}\frac{\partial u_\xi}{\partial \xi} + \frac{u_\eta}{H_\xi H_\eta}\frac{\partial H_\xi}{\partial \eta}\right)$$

$$\pi_{\eta\eta} = -p - \frac{2}{3}\mu\nabla\cdot\vec{u} + 2\mu\left(\frac{1}{H_\eta}\frac{\partial u_\eta}{\partial \eta} + \frac{u_\xi}{H_\xi H_\eta}\frac{\partial H_\eta}{\partial \xi}\right)$$

$$\pi_{\phi\phi} = -p - \frac{2}{3}\mu\nabla\cdot\vec{u} + 2\mu\left(\frac{u_\xi}{H_\xi H_\phi}\frac{\partial H_\phi}{\partial \xi} + \frac{u_\eta}{H_\eta H_\phi}\frac{\partial H_\phi}{\partial \eta}\right)$$

$$\begin{aligned} \pi_{\xi\eta} &= \pi_{\eta\xi} \\ &= \mu\left(\frac{1}{H_\eta}\frac{\partial u_\xi}{\partial \eta} + \frac{1}{H_\xi}\frac{\partial u_\eta}{\partial \xi} - \frac{u_\xi}{H_\xi H_\eta}\frac{\partial H_\xi}{\partial \eta} - \frac{u_\eta}{H_\xi H_\eta}\frac{\partial H_\eta}{\partial \xi}\right) \end{aligned}$$

$$\nabla\cdot\vec{u} = \frac{1}{H_\xi H_\eta H_\phi}\left\{\frac{\partial(H_\eta H_\phi u_\xi)}{\partial \xi} + \frac{\partial(H_\xi H_\phi u_\eta)}{\partial \eta}\right\}$$

Energy equation

$$\begin{aligned} &\rho Cp\left(\frac{u_\xi}{H_\xi}\frac{\partial T}{\partial \xi} + \frac{u_\eta}{H_\eta}\frac{\partial T}{\partial \eta}\right) \\ &\quad = \frac{1}{H_\xi H_\eta H_\phi}\left(\frac{\partial}{\partial \xi}\left(k\frac{H_\eta H_\phi}{H_\xi}\frac{\partial T}{\partial \xi}\right) + \frac{\partial}{\partial \eta}\left(k\frac{H_\xi H_\phi}{H_\eta}\frac{\partial T}{\partial \eta}\right)\right) \\ &\qquad - \frac{T}{\rho}\left(\frac{\partial \rho}{\partial T}\right)_p\left(\frac{u_\xi}{H_\xi}\frac{\partial p}{\partial \xi} + \frac{u_\eta}{H_\eta}\frac{\partial p}{\partial \eta}\right) \end{aligned} \tag{11}$$

where H_ξ, H_η, H_ϕ are the dimensional metric coefficients defined as

$$H_\xi = \sqrt{\left(\frac{\partial x}{\partial \xi}\right)^2 + \left(\frac{\partial y}{\partial \xi}\right)^2 + \left(\frac{\partial z}{\partial \xi}\right)^2}$$

$$H_\eta = \sqrt{\left(\frac{\partial x}{\partial \eta}\right)^2 + \left(\frac{\partial y}{\partial \eta}\right)^2 + \left(\frac{\partial z}{\partial \eta}\right)^2}$$

$$H_\phi = \sqrt{\left(\frac{\partial x}{\partial \phi}\right)^2 + \left(\frac{\partial y}{\partial \phi}\right)^2 + \left(\frac{\partial z}{\partial \phi}\right)^2}$$

Boundary conditions: The governing equations are subject to the following boundary conditions. At the particle surface, no-slip condition is applied and the temperature is specified. On the center line, symmetry conditions are imposed, i.e. η derivatives of temperature, pressure, and velocity, and η component of velocity are zero. At infinity, pressure, temperature, and uniform flow are specified.

The governing equations are discretized by a control volume technique. A power law scheme, based on Patankar's generalized formulation (Patankar, 1980), is employed to handle the convective–diffusive terms. Second order accurate, central differencing is applied to calculate H_ξ and H_η inside the computational domain, and first order accurate, forward or backward differencing is used at the domain boundaries.

A point successive under relaxation technique was used to solve the governing equations. The relaxation factor of 0.4 was adequate for the velocity, pressure and energy equations. The convergence criterion (maximum absolute error of the dependent variable between two successive iterations) in all test runs was set at 10^{-5}.

When calculating flow in complex geometries, the use of non-staggered grids offers considerable advantage over staggered grids because all variables are stored at the same location. However, a straightforward discretization can lead to checkerboard-type pressure variation due to pressure–velocity decoupling (Patankar, 1980). Recently, a method to eliminate this problem by introducing a smoothing pressure correction has been developed by Date (1996, 1998). This method is employed here with a non-staggered grid.

2.2. Model validation

In computational studies, it is vitally important that the computational model is validated using experimental data and/or semi-empirical correlations. Here the developed computational code has been validated by comparison with results for limiting cases that are available in the literature. These limiting cases include constant property flow over a sphere, constant property flow over an oblate and a prolate solid particle, and variable property flow over a sphere. Table 1 lists values for drag coefficient and Nusslet number for a spherical particle for different values of Reynolds number. The results are compared with values obtained from well-established correlations for drag coefficient and Nusselt number (Clift et al., 1978) and several recent studies (Feng and Michaelides, 2000; Balachandara and Ha, 2001). Predictions by both correlations and other numerical studies are accurate generally within ±3%. Drag coefficient and Nusslet number results for oblate and prolate particles exposed to a constant property flow are compared with values available in the literature (Comer and Kleinstreuer, 1995b; Chuchottaworn and Asano, 1986). The table shows that our computational model is able to predict the flow and heat transfer for non-spherical particles that is consistent with published results from literature. A number of correlations have been proposed to account for the property variations in predictions of Nusslet number for flow over a sphere. Young and Pfender (1987) have reported an extensive comparison of these correlations for a range of temperatures from 2000 K to 15,000 K for Reynolds number up to 100. At high temperatures (>8000 K), there is

Table 1
Comparison of results of present model with those available in literature

	Re_d ($U_\infty d/\nu$) = 20	Re_d ($U_\infty d/\nu$) = 50	Re_d ($U_\infty d/\nu$) = 100
Results for constant property flow over a sphere			
C_d (present model)	2.631	1.549	1.151
Clift et al. (1978)	2.71	1.57	1.10
Feng and Michaelides (2000)	2.68		1.09
Nu (present model)	4.135	5.364	6.950
Feng and Michaelides (2000)		5.40	6.96
Balachandara and Ha (2001)		5.40	6.91
Clift et al. (1978)	4.236	5.535	7.0
Results for constant property flow over oblate/prolate particles			
Nu for $b/a = 0.6$ (present model)	4.40	5.994	7.854
Nu (Comer and Kleinstreuer, 1995b)	4.36	6.00	7.64
Nu for $b/a = 1.4$ (present model)	3.687	4.844	6.222
Nu (Chuchottaworn and Asano, 1986)	3.78	4.94	6.25
Results for variable property plasma flow over a sphere			
Nu (present model)	3.618	5.11	
Sayegh and Gauvin (1979)	3.61	4.98	
Nu_f (present model)	4.572	6.383	8.381
Nu_f (Young and Pfender, 1987)	4.536	6.208	8.093

Nu_f is the Nusselt number based on thermal conductivity evaluated at film temperature.

considerable deviation between correlations, and this deviation increases with increasing far field temperature. At lower temperatures (⩽5000 K), there is close agreement between correlations. As such we have carried out a comparison at far field temperature of 5000 K with numerical results of Sayegh and Gauvin (1979) and empirical correlation recommended by Young and Pfender (1987). As seen from the tabulated results, our predictions agree well with published results and correlation. The forgoing comparisons with correlations, other numerical studies, and experimental data validate our computational model.

3. Results and discussion

To study the effect of Reynolds number, we have considered Reynolds number of 20, 50, and 100. Experimental measurements reported by Fincke et al. (1990) show that particle surface temperature is between 2000 and 3000 K for most of the particle residence time. To investigate the effect of particle surface temperature we have obtained results for 2000 K and 3000 K. For the far field, plasma temperatures of 5000–12,000 K are considered. To understand the effect of non-spherical particle shape, both oblate and prolate shapes are investigated. The shapes are represented in terms variations in the axis ratio from 1.6 (disk-like) to 0.4 (cylinder-like). Non-continuum, ionization, and evaporation effects are not considered in this study.

3.1. Effect of particle shape

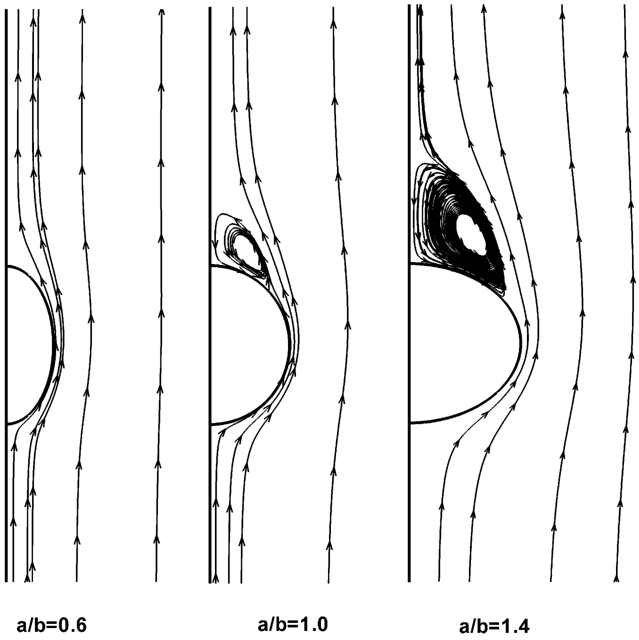

Fig. 1. Streamlines showing the effect of particle shape. $Re = 50$, $T_{\text{wall}} = 3000$ K, $T_{\infty} = 8000$ K, $a/b = 0.6$, 1, and 1.4.

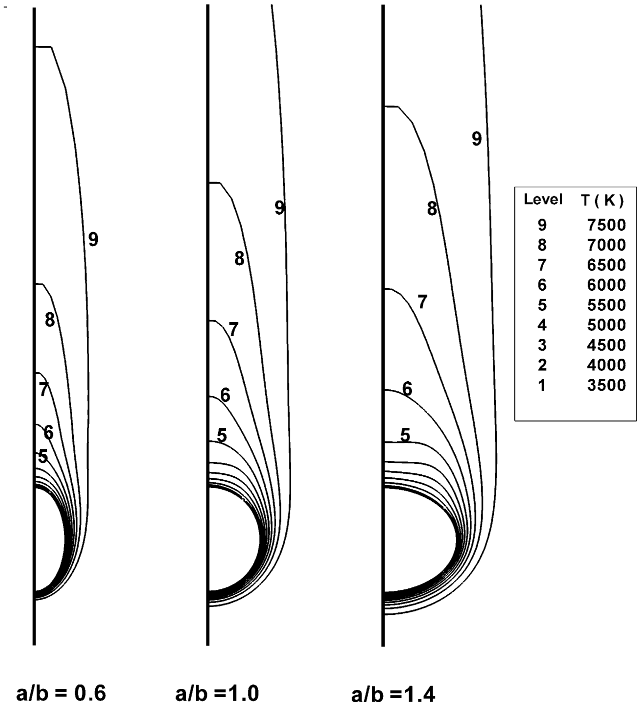

Fig. 2. Temperature contours. $Re = 50$, $T_{\text{wall}} = 3000$ K, $T_{\infty} = 8000$ K, $a/b = 0.6$, 1, and 1.4.

Fig. 1 shows the streamlines for flow over an oblate ($a/b = 1.4$), a spherical ($a/b = 1$), and a prolate ($a/b = 0.6$) particle at flow Reynolds number of 50. The corresponding temperature contours are plotted in Fig. 2. As the flow is considered axi-symmetric, only half of the flow domain is shown in the figures. As the fluid flows along the particle surface, there is flow separation at the rear of the particle with the streamlines showing a toroidal vortex flow pattern. An oblate particle provides the largest obstruction to the flow which results in a large re-circulating flow region near the rear stagnation point. A smaller re-circulating flow pattern is present for a spherical particle. As the hot fluid is brought towards the front stagnation point, for a prolate or a sphere, the gradients of velocity and temperature are likely to be the highest near the front stagnation point. However, for an oblate, the streamlines show that the gradients are likely to be the highest away from the centerline. This behavior is clearly evident in temperature contours shown in Fig. 2. Near the front stagnation point, due to the incoming flow at far field temperature, for the prolate and sphere, the temperature contours are most dense in that region. The density of the contours is proportional to the temperature gradient. In the rear part, the contours are spread apart. For the oblate particle, the temperature contours are also dense in the front part but the highest contour density is seen at a point away from the front stagnation point. For a prolate particle, the temperature gradient decreases monotonically along the particle surface from the front to the rear. However, due to the large re-circulation vortex in case of an oblate particle, the hot flow is brought closer to the particle surface at the rear and it results in increasing temperature gradients near the rear stagnation point. This behavior can be seen in Fig. 3 where the variation of local Nusslet number is plotted for a number of particle aspect ratios. Here, $\eta = 0$ corresponds to the front stagnation point and $\eta = 180$ indicates the rear stagnation point. At Reynolds number of 50, for prolate particles, the heat transfer coefficient is the highest near $\eta = 0$, and decreases monotonically along the particle surface. As the hot gases flow along the particle surface, due to heat transfer to the particle, the gas temperature decreases and thus the temperature gradient and consequently the heat transfer coefficient decreases. For a sphere, the behavior of heat transfer coefficient is similar to that of a prolate particle, except for $\eta > 140$. Due to the re-circulatory vortex at the rear, warmer fluid is brought closer to the particle surface and the heat transfer coefficient increases. This is more pronounced in case of an oblate particle with $a/b = 1.4$ where a significant increase in heat transfer coefficient is obtained for $\eta > 140$. As noted earlier, for an oblate particle, the temperature gradient and consequently local heat transfer coefficient is not the highest at $\eta = 0$ but occurs at around $\eta = 80$. Fig. 4 shows pressure variation along the particle surface. As the flow is brought to rest at the front stagnation point, the highest value of surface pressure is obtained at the front stagnation point. The pressure first decreases along the surface and then increases. The adverse pressure gradient is stronger in case of oblate particles, which leads to flow separation. The pressure has been made dimensionless by the free-stream momentum $(\rho U_\infty^2/2)$. At Reynolds number of 50, at the front stagnation point, the recovery of velocity head leads to dimensionless pressure closer to 1. At Reynolds number of 20, significant contribution due to viscous forces leads to the stagnation pressure being greater than 1. We note that at lower Reynolds number, the adverse pressure gradient is smaller and the flow does not separate.

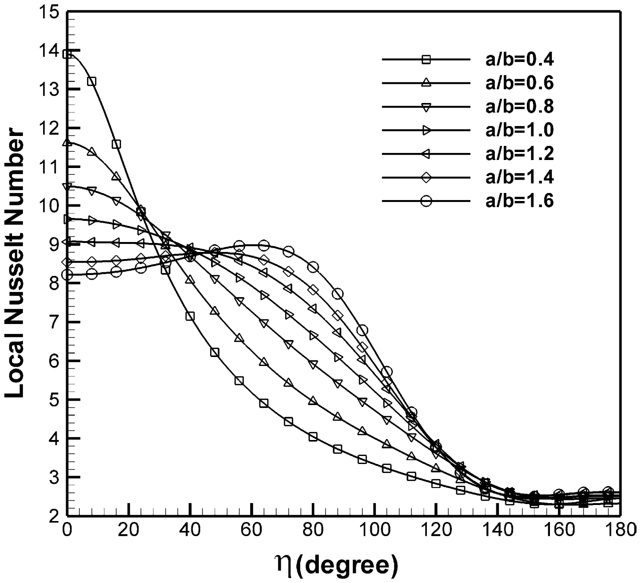

Fig. 3. Variation of local Nusselt number. $Re = 50$, $T_{\text{wall}} = 3000$ K, and $T_\infty = 5000$ K.

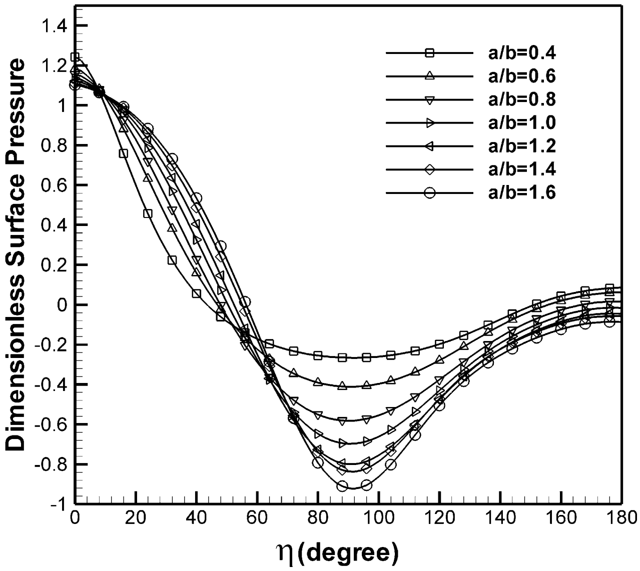

Fig. 4. Variation of dimensionless surface pressure. $Re = 50$, $T_{\text{wall}} = 3000$ K, and $T_\infty = 5000$ K.

3.2. Effect of Reynolds number

Flow streamlines for Reynolds number of 20, 50 and 100 are shown in Fig. 5 for an oblate particle (with

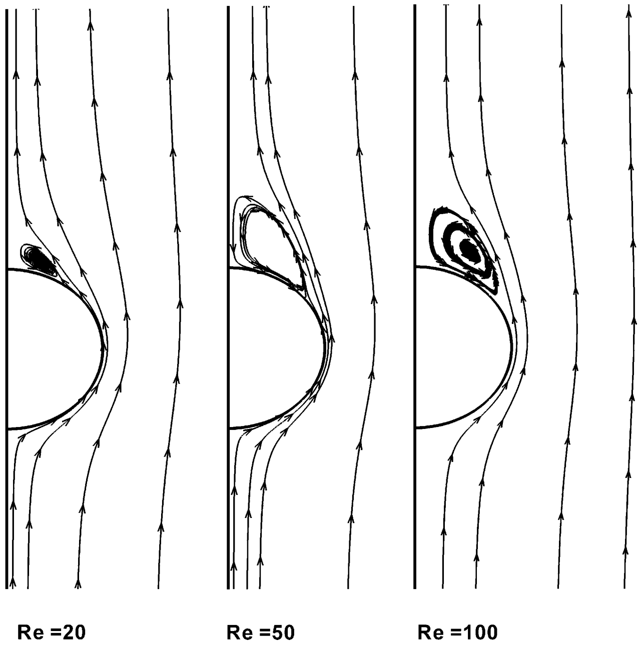

Fig. 5. Streamlines for flow over an oblate particle with $a/b = 1.2$, $T_{\text{wall}} = 2000$ K, $T_\infty = 8000$ K, for $Re = 20$, 50, and 100.

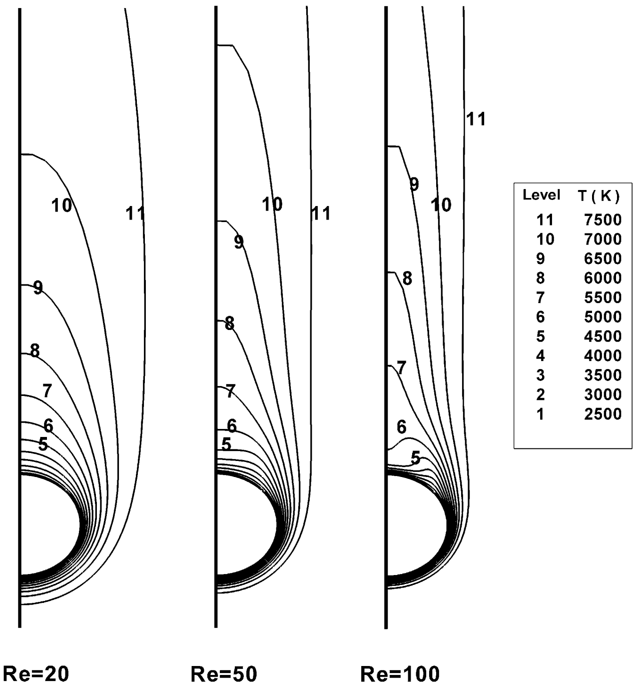

Fig. 6. Temperature contours for flow over an oblate particle with $a/b = 1.2$, $T_{\text{wall}} = 2000$ K, $T_\infty = 8000$ K, for $Re = 20$, 50, and 100.

$a/b = 1.2$). The corresponding temperature contours are shown in Fig. 6. For an oblate particle with $a/b = 1.2$, re-circulation at the rear of the particle is present for the entire range of Reynolds numbers considered here. It is seen that the size and strength of the re-circulation vortex increases with increasing Reynolds number. Fig. 6 shows that with increasing Reynolds number the temperature gradient close to the particle surface increases. This is to be expected as the hydrodynamic and thermal boundary layers become thinner with increasing Reynolds number. Due to re-circulation at the rear at higher Reynolds number, the temperature contours are pulled towards the particle surface. The large re-circulation vortex brings hot fluid closer to the particle surface, and consequently the temperature contours are seen to move closer to the particle surface. These effects are qualitatively similar to those reported for constant property flow (Comer and Kleinstreuer, 1995b; Chuchottaworn and Asano, 1986).

3.3. Effect of thermo-physical property variation

A comparison of flow streamlines for constant property flow with variable property flow is shown in Fig. 7 for an oblate particle. The predicted velocity gradients are greater when property variation is incorporated in

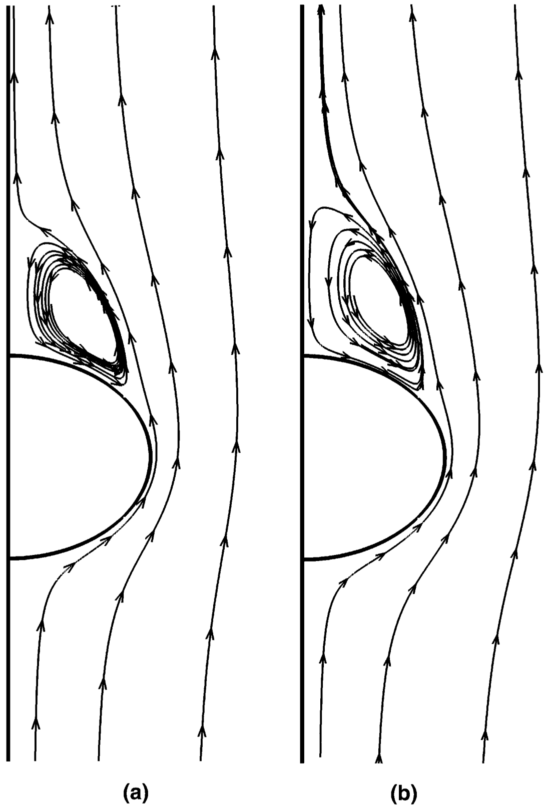

Fig. 7. Streamlines showing the effect of property variation for flow over an oblate particle. $Re = 50$, $a/b = 1.4$, $T_{\text{wall}} = 3000$ K, $T_\infty = 8000$ K. (a) Variable property flow and (b) constant property flow.

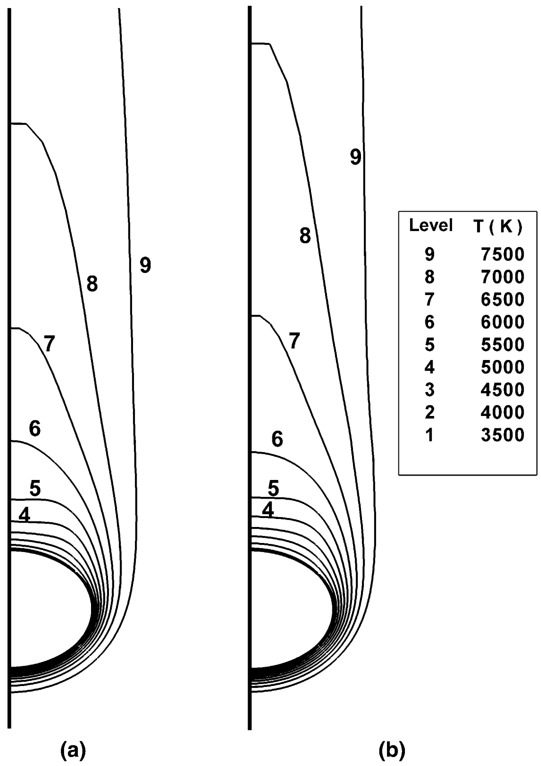

Fig. 8. Temperature contours showing the effect of property variation for flow over an oblate particle. $Re = 50$, $a/b = 1.4$, $T_{\text{wall}} = 3000$ K, $T_\infty = 8000$ K. (a) Variable property flow and (b) constant property flow.

the computations compared to those for constant property flow. The predicted re-circulation zone is larger for a constant property flow. The corresponding temperature contours are shown in Fig. 8. It is seen from the figure that accounting for property variation provides temperature contours that are closely spaced compared to those obtained with a constant property flow. This indicates that the predicted temperature gradient is significantly greater when property variation is considered in the computational model. With variable properties, the momentum and energy equations are coupled. For gases, thermal conductivity and viscosity are strong functions of temperature. A decrease in gas temperature results in lower viscosity and thermal conductivity. Therefore, with lower temperature in the vicinity of the particle surface compared to the free-stream, the

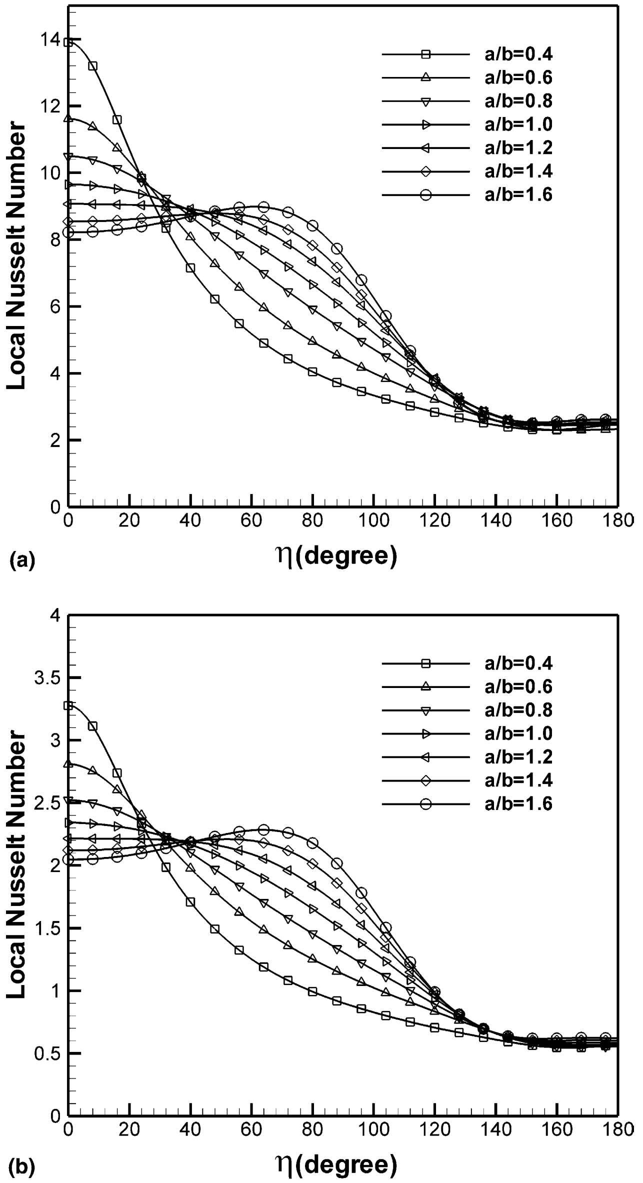

Fig. 9. Effect of property variation on the local Nusselt number. $Re = 50$. (a) $T_{\mathrm{wall}} = 3000$ K, $T_{\infty} = 5000$ K and (b) $T_{\mathrm{wall}} = 3000$ K, $T_{\infty} = 12{,}000$ K.

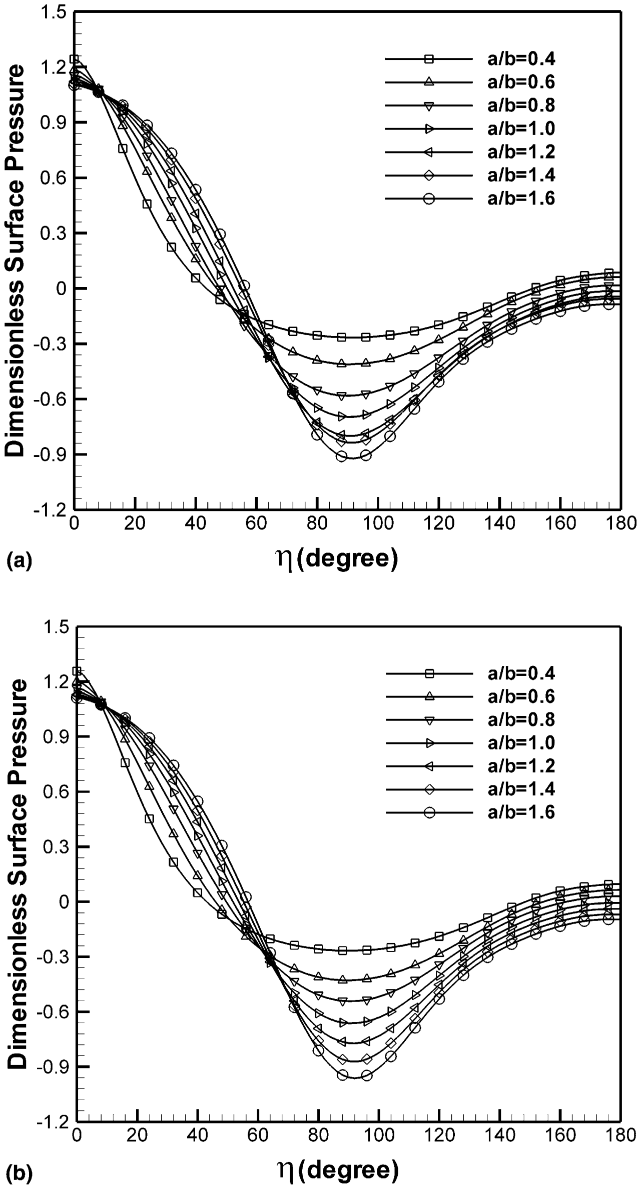

Fig. 10. Effect of property variation on the dimensionless surface pressure variation. $Re = 50$. (a) $T_{\mathrm{wall}} = 3000$ K, $T_{\infty} = 5000$ K and (b) $T_{\mathrm{wall}} = 3000$ K, $T_{\infty} = 12{,}000$ K.

Table 2
Particle surface temperature (T_{wall}) and free-stream temperature (T_{∞}) for each case

Case number	T_{wall} (K)	T_{∞} (K)
Case 1	3000	5000
Case 2	3000	8000
Case 3	3000	12,000
Case 4	2000	5000
Case 5	2000	8000
Case 6	2000	12,000

momentum diffusivity and thermal diffusivity are lower near the particle surface compared to the far field. Therefore the diffusion of momentum and energy is confined to a smaller radial distance compared to the constant property flow. This leads to higher velocity and temperature gradients with variable property flow.

The effects due to variable properties are further evident in Figs. 9 and 10 where local Nusselt number and surface pressure variations are shown for different far field temperatures. As the difference between particle surface temperature and far field temperature increases, the effect of property variation becomes more

Table 3
Results for Nusselt number based on thermal conductivity at the far field temperature

a/*b*	*Re*	Case 1	Case 2	Case 3	Case 4	Case 5	Case 6
0.4	20	2.743585	1.846511	0.781947	2.513813	1.694824	0.665291
	50	3.677111	2.50851	1.031007	3.522722	2.283969	0.860232
	100	4.880515	3.257861	1.308316	4.458036	2.948281	1.159386
0.6	20	3.131887	2.124492	0.913185	2.898642	1.963078	0.787227
	50	4.267096	2.924498	1.231604	4.079793	2.688985	1.02801
	100	5.570323	3.861053	1.559727	5.247349	3.503795	1.306797
0.8	20	3.410712	2.309518	1.008806	3.197308	2.152352	0.874779
	50	4.815814	3.184871	1.351598	4.47283	2.970926	1.150351
	100	6.15195	4.221954	1.739374	5.811249	3.923366	1.461723
1.0	20	3.617856	2.452686	1.080003	3.391633	2.28884	0.939378
	50	5.110055	3.430309	1.448783	4.755651	3.19612	1.241223
	100	6.584964	4.529036	1.871731	6.233882	4.227467	1.578279
1.2	20	3.769005	2.554366	1.133584	3.533324	2.388549	0.987691
	50	5.326737	3.543425	1.520298	4.960711	3.341888	1.308475
	100	6.91272	4.767425	1.971365	6.558158	4.465074	1.667602
1.4	20	3.882142	2.631965	1.173778	3.637053	2.461942	1.024236
	50	5.36832	3.653305	1.573312	5.111976	3.437015	1.363616
	100	7.305808	4.956723	2.048656	6.814964	4.65557	1.737816
1.6	20	3.971847	2.689508	1.204099	3.71236	2.51599	1.052014
	50	5.483624	3.73522	1.612951	5.225208	3.517623	1.400936
	100	7.515982	5.076148	2.109784	7.021276	4.779514	1.794204

Table 4
Results for drag coefficient

a/*b*	*Re*	Case 1	Case 2	Case 3	Case 4	Case 5	Case 6
0.4	20	3.266677	2.97466	3.127135	2.973372	2.752312	2.809206
	50	1.795371	1.647228	1.673269	1.66722	1.506738	1.48452
	100	1.184352	1.079636	1.067164	1.081163	0.979208	0.930161
0.6	20	2.666538	2.459993	2.629199	2.459222	2.296367	2.401864
	50	1.514275	1.395013	1.452017	1.415362	1.289891	1.308259
	100	1.017402	0.938846	0.9455	0.93691	0.85658	0.850973
0.8	20	2.331078	2.170756	2.328707	2.174726	2.030176	2.155344
	50	1.374716	1.253016	1.309875	1.268927	1.162623	1.202313
	100	0.929009	0.855878	0.876105	0.856725	0.791166	0.79946
1.0	20	2.102577	1.951985	2.115981	1.963149	1.845606	1.978569
	50	1.257594	1.158998	1.212781	1.165046	1.080739	1.125576
	100	0.865551	0.802695	0.827391	0.802421	0.746729	0.764192
1.2	20	1.950702	1.810386	1.950157	1.801216	1.703693	1.8383
	50	1.166073	1.072443	1.135194	1.085728	1.011991	1.063201
	100	0.819927	0.76309	0.788928	0.76305	0.714634	0.736278
1.4	20	1.802549	1.680067	1.81381	1.669421	1.587012	1.720841
	50	1.065871	1.008434	1.070233	1.01934	0.951528	1.012001
	100	0.785091	0.731264	0.756365	0.731039	0.6898	0.711879
1.6	20	1.679047	1.569214	1.696068	1.554762	1.48725	1.617505
	50	1.006082	0.953293	1.013346	0.96276	0.903176	0.964278
	100	0.751843	0.701798	0.727508	0.704445	0.667511	0.689501

significant. A very small temperature difference would mimic constant property flow solutions. Note that in the definition of Nusslet number thermal conductivity at T_∞ is used. Therefore, the Nusslet number values appear lower with higher free stream temperatures. As such the Nusselt number values in Fig. 9(b) (T_∞ = 12,000 K) are substantially lower than those in Fig. 9(a) (T_∞ = 5000 K). Furthermore, with far field temperature of 12,000 K, the difference in maximum local Nusselt number for $a/b = 1.4$ and for $a/b = 0.6$ is much smaller than that for far field temperature of 5000 K.

3.4. Correlation for average Nusselt number

Table 2 provides a matrix of temperature values considered to obtain numerical results. Tables 3 and 4 provide results for the average Nusslet number and the drag coefficient, respectively, for all particle shapes, Reynolds numbers, and temperatures considered in this study. We note that the Nusselt number is based on the thermal conductivity at the free stream temperature. As temperature increases, thermal conductivity increases for gases. Therefore, the Nusselt number values for high free stream temperature appear to be numerically very low. It is desirable to provide a simple way of expressing the effect of particle shape on transport for the range of Reynolds number considered here. For a constant property flow, such efforts to develop a simple correlation for the drag coefficient have not been successful as the effect on drag coefficient of particle shape is very sensitive to the value of the Reynolds number. In fact, it has been shown for constant property flow, that at Reynolds number >50, the effect may be opposite of that at lower Reynolds number. However, the effect of particle shape on Nusselt number is non-linear but monotonic and is not a function of Reynolds number within the range of Reynolds number considered here. The best fit for the variable property data for all the cases considered here gives

$$\frac{Nu}{Nu_{\mathrm{sphere}}} = \exp\left[-0.255\left(\frac{b}{a} - 1\right)\right]$$

This correlation deviates less than ±3% from the numerical solutions.

4. Conclusions

In this paper a numerical study of variable property plasma flow over spheroidal particles is presented. Results show that particle shape has significant effect on flow and heat transfer to particle surface. Within the range of Reynolds number considered here, for an oblate particle, a re-circulatory flow pattern is present at the rear of the particle and its strength and size increases as the Reynolds number increases. For a prolate particle, the flow does not separate at $Re = 20$ and the re-circulatory wake is much smaller than that for an oblate particle. Compared to a constant property flow, accounting for thermo-physical property variation leads to prediction of higher temperature and velocity gradients in the vicinity of the particle surface. Also with a variable property flow, the predicted size of the re-circulatory vortex is smaller. The results for drag coefficient and overall Nusselt number for non-spherical particles are substantially different from those for a sphere. The following correlation for the overall Nusselt number is presented for a variable property plasma flow to account for non-spherical particles shape that fits our numerical results within ±3%

$$\frac{Nu}{Nu_{\mathrm{sphere}}} = \exp\left[-0.255\left(\frac{b}{a} - 1\right)\right].$$

Acknowledgement

This work was supported by the National Science Foundation under grant # CTS-9733369.

References

Ayyaswamy, P.S., 1995. Direct contact transfer processes with moving droplets. In: Hartnett, J.P., Irvine, T.F. (Eds.), Advances in Heat Transfer, vol. 26. Academic Press, San Diego, CA, pp. 1–104.

Ayyaswamy, P.S., Cohen, I.M., 2002. Low energy plasma heat transfer as applied to microelectronic packaging. In: Tien, C.-L., Prasad, V., Incropera, F. (Eds.), Annual Review of Heat Transfer, vol. 12. Hemisphere Publication, New York.

Balachandara, S., Ha, M.Y., 2001. Unsteady heat transfer from a sphere in a uniform cross-flow. Physics of Fluids 13, 3714–3728.

Boulos, M.I., Fauchais, P., Pfender, E., 1994. Thermal Plasmas: Fundamentals and Applications, vol. 1. Plenum Press.

Bourdin, E., Fauchais, P., Boulos, M., 1983. Transient heat conduction under plasma conditions. Int. J. Heat Mass Transfer 26, 567–582.

Chen, X., 1997. Heat transfer to a metallic wire exposed to a plasma flow for great Knudsen numbers. J. Phys. D: Appl. Phys. 30, 1885–1892.

Chen, X., Chen, J., Wang, Y., 1994. Heat transfer from a rarefied plasma flow to a metallic particle with high surface temperature. J. Phys. D: Appl. Phys. 27, 1637–1645.

Chyou, Y.P., Pfender, E., 1989. Behavior of particulates in thermal plasma flows. Plasma Chem. Plasma Process. 9, 45–71.

Clift, R., Grace, J.R., Weber, M.E., 1978. Bubbles, Drops and Particles. Academic Press.

Comer, J.K., Kleinstreuer, C., 1995a. A numerical investigation of laminar flow past nonspherical solids and droplets. J. Fluids Eng. 117, 170–175.

Comer, J.K., Kleinstreuer, C., 1995b. Computational analysis of convection heat transfer to non-spherical particles. Int. J. Heat Mass Transfer 38 (17), 3171–3180.

Chuchottaworn, P., Asano, K., 1986. Numerical analysis of drag coefficients and the heat and mass transfer of spherical drops. J. Chem. Eng. Jpn. 19 (3), 208–213.

Date, A.W., 1996. Complete pressure correction algorithm for solution of incompressible Navier–Stokes equations on a non-staggered grid. Numer. Heat Transfer Part B 29, 441–458.

Date, A.W., 1998. Solution of Navier–Stokes equations on non-staggered grid at all speeds. Numer. Heat Transfer Part B 33, 451–467.

Eca, L., 1996. 2D orthogonal grid generation with boundary point distribution control. J. Comput. Phys. 125, 440–453.

Feng, Z.G., Michaelides, E.E., 2000. A numerical study on the transient heat transfer from a sphere at high Reynolds and Peclet numbers. Int. J. Heat Mass Transfer 43, 219–229.

Fincke, J.R., Swank, W.D., Jeffery, C.L., 1990. Simultaneous measurement of particle size, velocity, and temperature in thermal plasma. IEEE Trans. Plasma Sci. 18, 948–957.

Gnedovets, A.G., Uglov, A.A., 1992. Heat transfer to nonspherical particles in a rarefied plasma flow. Plasma Chem. Plasma Process. 12, 383–401.

Hader, M.A., Jog, M.A., 1998. Continuum plasma flow past a sphere. Phys. Plasmas 5 (4), 902–909.

Jog, M.A., Huang, L., 1996. Transient heating and melting of particles in plasma coating process. J. Heat Transfer 118, 471–477.

Joshi, S.V., Park, J.Y., Taylor, P.R., Richardson, L.S., 1986. Particle–gas mass transfer under plasma conditions. Int. J. Heat Mass Transfer 29, 1565–1573.

Masliyah, J.H., Epstein, N., 1970. Numerical study of steady flow past spheroids. J. Fluid Mech. 44 (part3), 513–528.

Patankar, S.V., 1980. Numerical Heat Transfer and Fluid Flow. Hemisphere Publishing, Washington.

Sadhal, S.S., Ayyaswamy, P.S., Chung, J.N., 1997. Transport Phenomena with Bubbles and Drops. Springer-Verlag.

Sayegh, N.N., Gauvin, W.H., 1979. Numerical analysis of variable property heat transfer to a single sphere in high temperature surroundings. AIChe J. 25, 522–534.

Smith, R.W., Wei, D., Apelian, D., 1989. Thermal plasma materials processing. Plasma Chem. Plasma Process. 9, 135S–165S.

Thompson, J.F., Warsi, Z.U.A., 1982. Boundary-fitted coordinate systems for numerical solution of partial differential equations—a review. J. Comput. Phys. 47, 1–108.

Verma, A., Jog, M.A., 2000. Plasma flow over an array of particles. Int. J. Heat Mass Transfer 43, 101–111.

Wen, Y., 2004. Numerical study of variable property plasma flow over non-spherical particles. M.S. Thesis, University of Cincinnati.

Young, R.M., Pfender, E., 1987. Nusselt number correlations for heat transfer to small spheres in thermal plasma flows. Plasma Chem. Plasma Process. 7 (2), 211–226.